

Metamagnetism in La_2CuO_4

S-W. Cheong, J. D. Thompson, and Z. Fisk

Los Alamos National Laboratory, Los Alamos, New Mexico 87545

(Received 19 September 1988)

A careful study of the metamagnetic transition in single-crystalline La_2CuO_4 is presented. From magnetic susceptibility measurements the critical exponent (β) of the weak ferromagnetic state, which terminates at a triple point, has been estimated to be $\beta=0.5\pm 0.02$, a value consistent with mean-field theory. Furthermore, the pressure dependence of the critical magnetic field for the transition has been examined from magnetoresistance measurements under hydrostatic pressure.

The magnetic properties of La_2CuO_4 have been examined in detail,¹⁻⁴ particularly in an attempt to understand any possible interrelationship between magnetism found in La_2CuO_4 and superconductivity in La_2CuO_4 -based compounds. An anomaly in the susceptibility¹ of La_2CuO_4 suggested the presence of an antiferromagnetic phase transition, which has been confirmed by neutron-scattering experiments that find three-dimensional Bragg peaks with unit-cell coupling. The Néel temperature (T_N) is extremely sensitive to the oxygen content.¹ Neutron-scattering experiments² have also established the existence of strong two-dimensional (2D) magnetic correlations even far above T_N ; in addition, two-magnon Raman scattering experiments³ show the presence of strong, magnetic intralayer coupling. Furthermore, a field-induced transition,⁴ which occurs when a magnetic field is applied perpendicular to the CuO planes at a temperature below T_N , has been reported. The origin of this metamagnetic, field-induced transition is from the canting of Cu spins out of the CuO planes due to the rotational distortion of elongated octahedra of oxygen atoms around the divalent Cu ions. The susceptibility peak around T_N has been attributed to antiferromagnetic ordering in the presence of the Dzyaloshinski-Moriya interaction⁵ which is allowed by the distorted coordination of oxygen atoms.

Since the critical behavior around the Néel temperature has not been explored in detail, and the driving force producing the Néel state has not been established well, we have performed careful measurements of the magnetic susceptibility (χ)/magnetization around T_N on a crystal of La_2CuO_4 which exhibits a very sharp susceptibility peak, indicative of a well-ordered homogeneous sample.

Large crystals of La_2CuO_4 (as large as $3\times 3\times 0.3\text{ cm}^3$) were grown from a CuO flux. After quenching from high temperatures, crystals were removed from the CuO flux and annealed in an appropriate gas atmosphere according to the oxygen content desired. We found that proper annealing is necessary to ensure a sharp magnetic transition and, furthermore, reduces the temperature-independent background in χ , as well as suppresses the low-temperature Curie-tail frequently observed in less well-ordered samples. We observed the peak temperature (T_p) in χ as high as 326 K in crystals annealed in a nitro-

gen atmosphere. The distinction between T_N and T_p will be discussed herein. The data shown here are representative of crystals annealed in air with $T_p\sim 257\text{ K}$. Susceptibility and magnetization were measured with a Quantum Design superconducting-quantum-interference-device susceptometer capable of magnetic fields to 5 T.

The temperature-dependent magnetic susceptibility of a La_2CuO_4 crystal, measured in 0.2-T magnetic field applied in the CuO-plane direction (χ_{\parallel}) and in the perpendicular direction (χ_{\perp}), is displayed in the left panel of Fig. 1. Even though divalent Cu ions are good Heisenberg ions, because of large spin-orbit coupling and the fact that the ground state is a Kramer's doublet, there is appreciable susceptibility anisotropy. χ_{\perp} shows a sharper peak, with $T_p=257\pm 0.5\text{ K}$, than χ_{\parallel} and the full width at half maximum of the peak is $\sim 13\text{ K}$, indicating good homogeneity of oxygen distribution in the sample. The right panel in Fig. 1 exhibits the magnetic field dependence of χ_{\perp} (0.2 T data are the same as shown in the left panel). A clear difference in the two susceptibility curves is evident. We note that in the case of χ_{\parallel} there is no field dependence except for a slight depression of T_p .

In Fig. 2, we plot isothermal magnetization curves at various temperatures with the applied field perpendicular to the CuO planes. As reported earlier,⁴ the field-induced transition, indicated by the deviation from linear $M(H)$ behavior found for $T < T_p$, shifts to lower-field values with increasing temperature. Above T_p , $M(H)$ curves are linear with a slight tendency toward saturation at high-field values. However, it is not clear, from data like these, precisely at what temperature the jump in $M(H)$ curves disappears. The inset will be discussed later.

The critical fields (H_c), defined from the maximum of $|dM/dH|$, as a function of temperature are plotted in the left panel of Fig. 3. The right panel displays the temperature dependence of the jump (M_s) in $M(H)$ curves at the critical field—values of M_s were determined by the difference at H_c between smooth extrapolations of low-field and high-field portions of the $M(H)$ curves. We found from careful analysis that $H_c(T)$ does not extrapolate smoothly to zero at $T_p=257\pm 0.5\text{ K}$ and that M_s extrapolates to zero at $T=251.5\pm 0.5\text{ K}$. This behavior has been observed in a number of samples that show a

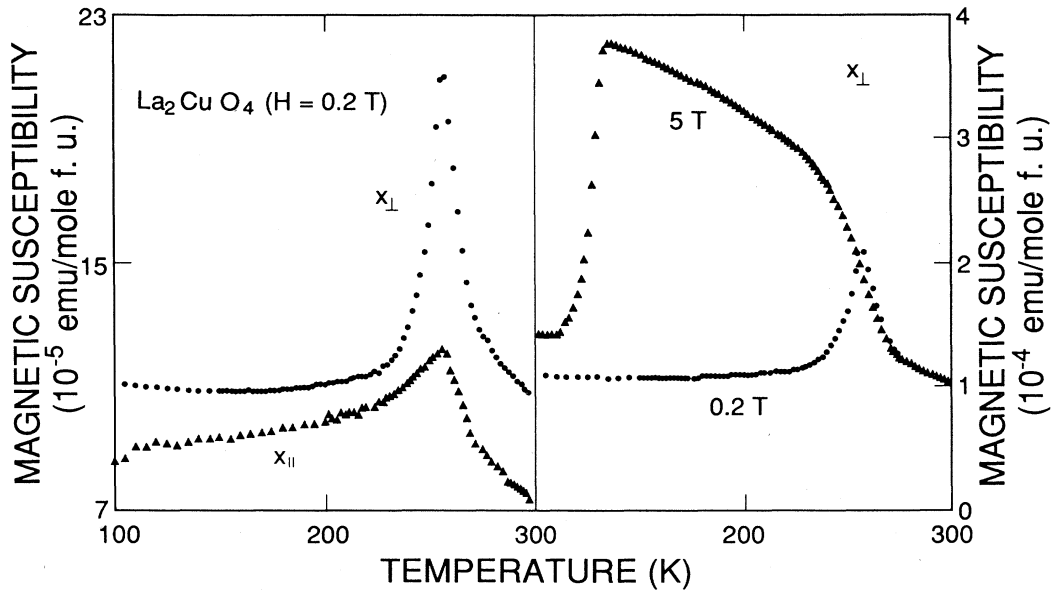


FIG. 1. The left panel displays temperature dependence of the magnetic susceptibility of La_2CuO_4 in the CuO plane direction (χ_{\parallel}) and in the perpendicular direction (χ_{\perp}) measured with 0.2-T field. The χ_{\perp} vs temperature measured with two different fields (0.2 and 5 T) is shown in the right panel (0.2-T data are the same as those shown in the left panel). f.u. denotes formula unit.

susceptibility peak at different temperatures because of differing oxygen content. The temperature T_p does not necessarily define the Néel temperature and, in fact, the correct definition of T_N is not simple; however, there are arguments⁶ that the temperature variation of the specific heat of an antiferromagnet is essentially the same as that of the temperature derivative of the susceptibility, i.e., $C(T) = A(\partial/\partial T)[T\chi(T)]$, where A is a slowly varying function of temperature. Using this, we propose the phase diagram shown in the left panel of Fig. 3 where we have defined the Néel temperature as the temperature where $\partial/\partial T[T\chi_{\perp}(T)]$ reaches its maximum: we find

$$T_N(H \approx 0) = 253 \pm 0.5 \text{ K}.$$

The triple-point temperature ($T_t = 251.5 \pm 0.5 \text{ K}$) is estimated from the extrapolation of M_s to zero, shown in the right panel of Fig. 3. In an ideal sample the jump in $M(H)$ should disappear at this temperature. The critical field at T_t is estimated to be $2.05 \pm 0.05 \text{ T}$ from a smooth extrapolation of the curve shown in the left panel of Fig. 3. We note that M_s also extrapolates to zero at $H_c = 2.05 \pm 0.05 \text{ T}$ in a plot of M_s versus H_c at various temperatures. The phase diagram shown in the left panel of Fig. 3 has been constructed as follows: the antiferro-

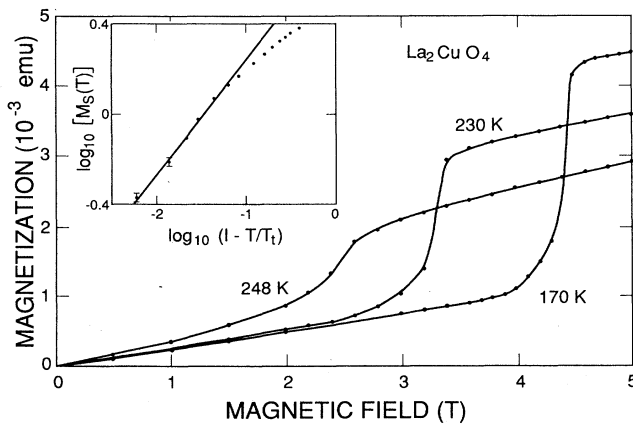


FIG. 2. Isothermal magnetization vs field at various fixed temperatures (sample mass = 105.1 mg). The inset shows $\log_{10} M_s$ vs $\log_{10}(1 - T/T_t)$ from which we deduce $M_s \propto (1 - T/T_t)^{0.5}$.

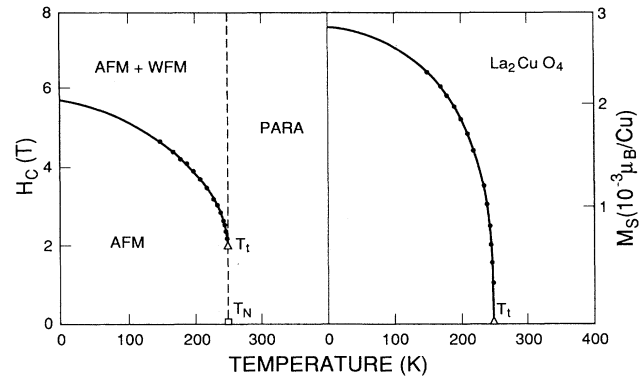


FIG. 3. The left panel: Field-temperature phase diagram deduced from magnetization measurements ($T_N = 253 \pm 0.5 \text{ K}$, $T_t = 251.5 \pm 0.5 \text{ K}$). The right panel: M_s vs temperature, where M_s is the jump in isothermal magnetization curves.

magnetic and paramagnetic states are divided by the straight, dashed line connecting points ($T_N=253$ K, 0 T) and ($T_t=251.5$ K, 2.05 T), and the boundary defined by connecting the critical-field points distinguishes the low-field antiferromagnetic (AFM) state and the high-field state [AFM + weak ferromagnetic (WFM)] in which antiferromagnetism and weak ferromagnetism coexist. The two phase boundaries meet at the triple point where M_s vanishes. When a field less than 2.05 T is applied, the shape of the susceptibility peak does not change and T_p moves down slowly with increasing field ($\partial T_p/\partial H \sim -0.8$ K/T), which supports our suggestion. Though not shown here, small hysteresis is observed in magnetoresistance and magnetization measurements when crossing the $H_c(T)$ phase boundary, with the hysteresis becoming more pronounced at temperatures far below T_N . This would suggest that the boundary between AFM and AFM+WFM may be first order or at least weakly first order. We point out that the presence of a tricritical point in other metamagnets,⁷ e.g., FeCl_2 , could indicate that the triple point discussed earlier is a tricritical point below which a first-order transition occurs and, otherwise, the transition is second order.

Using the proposed phase diagram shown in the left panel of Fig. 3, we can investigate the critical behavior of weak ferromagnetism around the triple point. As shown in the inset of Fig. 2, in the temperature range 235 K $< T < 250$ K, the spontaneous magnetization, which we assume to be identical to the magnetization jump (M_s), follows

$$M_s(T) \propto (1 - T/T_t)^\beta,$$

where $T_t=251.5$ K and $\beta=0.5 \pm 0.02$. However, there is a clear, smooth deviation from the above relation below 230 K. In mean-field theory, the critical exponent (β) has been estimated to be 0.5 and verified experimentally in other weak ferromagnetic systems,⁸ e.g., MnCO_3 or CoCO_3 . The agreement between predictions of mean-field theory and the observed value of β in La_2CuO_4 , together with the reasonably large interlayer coupling (see the following) in La_2CuO_4 , is consistent with the three-dimensional character of magnetic order in La_2CuO_4 observed by neutron scattering. This is in contrast with the critical exponent (β) of antiferromagnetism determined by neutron-scattering experiments in the 2D magnet K_2NiF_4 , in which β is found to be equal to 0.138 and close to the 2D Ising model prediction.⁹

In studying several samples with varying amounts of oxygen, we have found that the magnitude of $H_c(T)$ scales approximately as T_N . Preliminary measurements¹⁰ of the electrical resistivity of La_2CuO_4 sintered samples subjected to moderate hydrostatic pressures reveals a volume dependence of T_N that in turn, then, might suggest a volume dependence of $H_c(T)$. To investigate this possibility, we have performed magnetoresistance measurements at liquid-nitrogen temperature on a single crystal of La_2CuO_4 having a slightly lower T_N and correspondingly lower critical field than the crystal on which susceptibility data are shown in Figs. 1–3. As reported earlier,⁴ a large negative magnetoresistance develops, for

fields applied perpendicular to the CuO planes, when crossing the boundary separating the AFM and AFM+WFM phases. Results obtained at two pressures are shown in Fig. 4. With increasing pressure the magnetoresistance change at H_c diminishes and the critical field decreases. The inset of Fig. 4 summarizes the effect of pressure on H_c at 75 K. If we assume that H_c scales with T_N , then we should expect

$$\partial \ln T_N / \partial P = \partial \ln H_c / \partial P \simeq -0.4\% / \text{kbar},$$

a value in qualitative agreement with direct measurements¹¹ of $T_N(P)$. We note that Fisher *et al.*¹² estimated $\partial \ln J / \partial P \sim 0.2\% / \text{kbar}$; however, the relation between J and T_N is not clear. Finally, we note that the large magnetoresistance change at H_c implies a strong correlation between magnetism and transport in La_2CuO_4 . This correlation persists in zero-applied magnetic field where a decrease¹³ in the out-of-plane resistivity by nearly 70% is found in cooling from above T_N . Although the in-plane resistivity also decreases below T_N , it is not so pronounced. Such a large change ($\Delta\rho$ of order $10 \Omega \text{ cm}$) is clearly much greater than expected from simple spin-disorder scattering.

As discussed in the introduction, the Dzyaloshinski-Moriya (D-M) interaction arising from the rotationally-distorted octahedral coordination of oxygens around Cu^{+2} ions is probably responsible for the field-induced transition. The canting of spins out of each CuO layer, arising from the D-M interaction, produces a net moment perpendicular to the CuO planes. At low magnetic fields, however, the spins in alternate layers cant in opposite directions and the net moment in one layer cancels that in the next layer. (That the crystal structure is face-C centered is an important factor in producing this situation.) However, when a high enough magnetic field is applied perpendicular to the CuO planes, the net moment in each layer points in the magnetic field direction and produces a weak ferromagnetic moment. The effective ex-

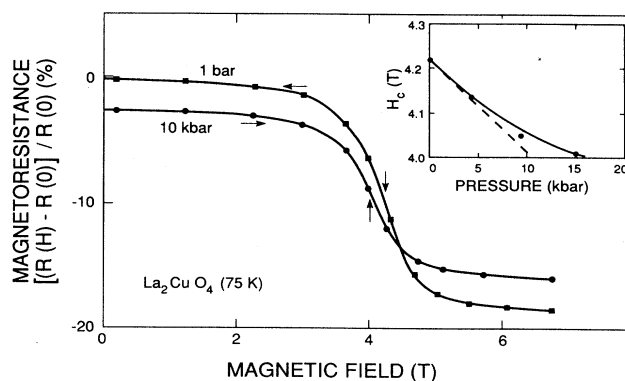


FIG. 4. Magnetoresistance vs field at 75 K for two different pressures. The inset displays H_c versus pressure, where H_c is defined from the maximum of $|dR(H)/dH|$. This sample exhibited a lower T_N and H_c than found in the sample used for magnetization measurements.

change Hamiltonian, including the D-M interaction, is given by

$$H_{\text{ex}} = 2 \sum_{i>j} (J_{ij} \mathbf{S}_i \cdot \mathbf{S}_j + \mathbf{D}_{ij} \cdot \mathbf{S}_i \times \mathbf{S}_j). \quad (1)$$

Assuming a classical spin model at zero temperature, we can relate the canting angle (θ) of Cu^{2+} spins out of the CuO planes with exchange parameters by expanding the above Hamiltonian up to θ^2 and maximizing the energy gain in the ordered state, giving

$$\theta = \frac{D}{2J} = \frac{M_s(0)}{g\mu_B S}, \quad (2)$$

where J is the intralayer superexchange coupling and $\mathbf{D} = (D, 0, 0)$.

By extrapolating $H_c(T)$ and $M_s(T)$ to zero temperature as shown in Fig. 3, we estimate $H_c(0) = 5.7$ T and $M_s(0) = 2.8 \times 10^{-3} \mu_B/\text{Cu}$. From two-magnon Raman scattering experiments,³ J is estimated to be equal to 675 K. In using Eq. (2), i.e., $T \ll T_N$, we must also take into account reduction¹⁴ of the spin $\frac{1}{2}$ due to two-dimensionality, which is predicted to be $\sim 35\%$ from spin-wave theory. With these values, Eq. (2) gives $\theta = 3.9 \times 10^{-3}$ rad and $D = 5.3$ K ($g = 2.2$ has been used¹⁵). It is interesting to compare the obtained value of θ with the angle of rotational distortion of oxygen-octahedral coordination, which was observed to be 0.048 rad.¹⁶

By including a Zeeman term to the exchange Hamiltonian [Eq. (1)], and computing the competition between the Zeeman term and interlayer coupling in field, we can relate the interlayer coupling (J_{\perp}) with the observed parameters

$$J_{\perp} = \frac{g\mu_B \theta H_c(0)}{4S} = \frac{M_s(0)H_c(0)}{4S^2},$$

giving $J_{\perp} \sim 0.025$ K. Thus, the ratio between interlayer coupling and intralayer coupling is $\sim 3.7 \times 10^{-5}$ in La_2CuO_4 and is about one order of magnitude larger than in two-dimensional magnets,¹⁷ e.g., K_2NiF_4 , suggesting that ordering is induced by interlayer coupling in La_2CuO_4 . We reiterate that samples with higher T_N show larger values of $M_s(0)$ and $H_c(0)$, i.e., larger interlayer coupling, supporting the preceding suggestion.

In summary, we have studied the magnetic behavior of La_2CuO_4 and estimated the ratio between interlayer and intralayer coupling and the critical exponent (β) for the weak ferromagnetic state. Together these suggest that magnetic ordering exhibits three-dimensional character and that the Néel state is driven by interlayer exchange coupling. We also examined the pressure dependence of the field-induced transition in La_2CuO_4 which indicates that

$$\partial \ln T_N / \partial P = \partial \ln H_c / \partial P \approx -0.4\% / \text{kbar}.$$

- ¹D. C. Johnston, S. K. Sinha, A. J. Jacobson, and J. M. Newsam, *Physica B* (to be published).
- ²G. Shirane, Y. Endoh, R. J. Birgeneau, M. A. Kastner, Y. Hidaka, M. Oda, M. Suzuki, and T. Murakami, *Phys. Rev. Lett.* **59**, 1613 (1987).
- ³K. B. Lyons, P. A. Fleury, J. P. Remeika, and T. J. Negran, *Phys. Rev. B* **37**, 2353 (1988).
- ⁴S-W. Cheong, Z. Fisk, J. O. Willis, S. E. Brown, J. D. Thompson, J. P. Remeika, A. S. Cooper, R. M. Aikin, D. Schiferl, and G. Gruner, *Solid State Commun.* **65**, 111 (1988); S-W. Cheong, J. D. Thompson, Z. Fisk, and G. Gruner, *Solid State Commun.* **66**, 1019 (1988); T. Thio, T. R. Thurston, N. W. Preyer, P. J. Picone, M. A. Kastner, H. P. Jensen, D. R. Gaabe, C. Y. Chen, R. J. Birgeneau, and A. Aharony, *Phys. Rev. B* **38**, 905 (1988).
- ⁵I. Dzyaloshinski, *J. Phys. Chem. Solids* **4**, 241 (1958); T. Moriya, *Phys. Rev.* **120**, 91 (1960).
- ⁶M. E. Fisher, *Proc. Roy. Soc. (London) A* **254**, 66 (1960); M. E. Fisher, *Philos. Mag.* **7**, 1731 (1962).
- ⁷I. S. Jacobs and P. E. Lawrence, *Phys. Rev.* **164**, 866 (1967).
- ⁸A. S. Borovik-Romanov, *Zh. Eksp. Teor. Fiz.* **36**, 766 (1959) [*Sov. Phys.—JETP* **9**, 539 (1959)]; A. S. Borovik-Romanov and V. I. Ozogin, *Zh. Eksp. Teor. Fiz.* **39**, 27 (1960) [*Sov. Phys.—JETP* **12**, 18 (1961)].
- ⁹R. J. Birgeneau, J. Skalyo, Jr., and G. Shirane, *J. Appl. Phys.* **41**, 1303 (1970).
- ¹⁰H. A. Borges, R. S. Kwok, Z. Fisk, J. D. Thompson, M. McElfresh, S. Horn, and S. A. Shaheen, *Bull. Am. Phys. Soc.* **33**, 473 (1988).
- ¹¹M. C. Aronson, J. D. Thompson, S-W. Cheong, and Z. Fisk (unpublished).
- ¹²D. S. Fisher, A. J. Millis, P. Shraiman, and R. N. Bhatt, *Phys. Rev. Lett.* **61**, 482 (1988).
- ¹³S-W. Cheong, J. D. Thompson, Z. Fisk, and G. Gruner (unpublished).
- ¹⁴L. H. de Jongh, *Solid State Commun.* **65**, 963 (1988); R. Navarro, H. Algra, L. J. de Jongh, R. L. Carlin, and C. J. O'Connor, *Physica* **86-88B**, 693 (1977).
- ¹⁵H. Thomann, D. C. Johnston, P. J. Tindall, D. P. Goshorn, and R. A. Klemm (unpublished).
- ¹⁶Von B. Grande, H. K. Muller-Buschbaum, and M. Schweizer, *Z. Anorg. Allg. Chem.* **428**, 120 (1977).
- ¹⁷L. J. de Jongh and A. R. Miedema, *Adv. Phys.* **23**, 1 (1974).